Microfluid Nanofluid
DOI 10.1007/s10404-010-0660-x

RESEARCH PAPER

Modeling and high performance simulation of electrophoretic techniques in microfluidic chips

Pablo A. Kler · Claudio L. A. Berli · Fabio A. Guarnieri

Received: 1 April 2010 / Accepted: 20 June 2010

Abstract Electrophoretic separations comprise a group of analytical techniques such as capillary zone electrophoresis, isoelectric focusing, isotachophoresis, and free flow electrophoresis. These techniques have been miniaturized in the last years and now represent one of the most important applications of the lab-on-a-chip technology. A 3D and time-dependent numerical model of electrophoresis on microfluidic devices is presented. The model is based on the set of equations that governs electrical phenomena, fluid dynamics, mass transport, and chemical reactions. The relationship between the buffer characteristics (ionic strength and pH) and surface potential of channel walls is taken into consideration. Numerical calculations were performed by using PETSc-FEM, in a Python environment, employing high performance parallel computing. The method includes a set of last generation preconditioners and solvers, especially addressed to 3D microfluidic problems, which significantly improve the numerical efficiency in comparison with typical commercial software for multiphysics. In this work, after discussing two validation examples, the numerical prototyping of a microfluidic chip for two-dimensional electrophoresis is presented.

Keywords Microfluidic chips · Electrophoresis · Numerical model · PETSc-FEM

1 Introduction

Electrophoretic separation techniques are based on the mobility of ions under the action of an external electric field. These techniques, which are widely used in chemical and biochemical analysis, have been miniaturized in the last 20 years and now represent one of the most important applications of lab-on-a-chip (LOC) technology (Manz et al. 1990; Landers 2007; Tian and Finehout 2008). Electrophoretic separations carried out by LOC technology comprise a group of different techniques such as capillary zone electrophoresis (CZE), isoelectric focusing (IEF), isotachophoresis (ITP), moving boundary electrophoresis (MBE), and free flow electrophoresis (FFE) (Reyes et al. 2002; Peng et al. 2008; Wu et al. 2008). CZE, MBE, and ITP are based on the displacement of electrophoretic species along the microchannel. IEF allows amphoteric component to focus at its stable isoelectric point (p*I*) in a predefined pH gradient (Sommer and Hatch 2009). Free flow methods, such as FFE or free flow IEF (FFIEF), employ transverse electric fields in relation to the flow

Electronic supplementary material The online version of this article (doi:10.1007/s10404-010-0660-x) contains supplementary material, which is available to authorized users.

P. A. Kler (✉) · C. L. A. Berli · F. A. Guarnieri
CIMEC, INTEC (UNL-CONICET), Güemes 3450,
3000 Santa Fe, Argentina
e-mail: pkler@intec.unl.edu.ar

C. L. A. Berli
e-mail: cberli@santafe-conicet.gov.ar

F. A. Guarnieri
e-mail: aguarni@santafe-conicet.gov.ar

C. L. A. Berli
Dpto. Físico Matemática, FICH, UNL, Ciudad Universitaria,
3000 Santa Fe, Argentina

F. A. Guarnieri
Fac. de Bioingeniería, UNER, Oro Verde, Argentina

Published online: 09 July 2010

direction, allowing continuous operation and the possibility of connecting a second electrophoretic method. In fact, two-dimensional electrophoresis (2DE) are very demanded in proteins studies (Xu et al. 2005; Kohlheyer et al. 2008; Turgeon and Bowser 2009). As microchips for electrophoresis are becoming increasingly complex, simulation tools are required to numerically prototype the devices, as well as to control and optimize manipulations (Erickson 2005).

The first mathematical model of electrophoresis was developed by Saville and Palusinski (1986). This 1D model is valid for monovalent analytes in a stagnant electrolyte solution, without electro-osmotic flow (EOF). More complex models of conventional electrophoresis were later reported (Hruska et al. 2006; Thormann et al. 2007; Bercovici et al. 2009). Numerical simulations aimed to LOC technology involving fluid flow and species transport were early addressed to electrokinetic focusing and sample dispensing techniques (Patankar and Hu 1998; Ermakov et al. 1998, 2000), by employing an algorithm based on finite volume method in a structured grid. Bianchi et al. (2000) performed 2D finite element method (FEM) simulations of EOF in T-shaped microchannels, taking into account the inner part of the electric double layer (EDL). Arnaud et al. (2002) developed a FEM simulation of IEF for 10 species, without considering migration nor convection. Chatterjee (2003) developed a 3D finite volume model to study several applications in microfluidics. More recently, Barz (2009) developed a fully coupled model for electrokinetic flow and migration in microfluidic devices employing 2D FEM. Different simulations of electrophoretic separations based on IEF techniques were presented by Hruska et al. (2006) and Thormann et al. (2007) in 1D domains, and by Shim et al. (2007) and Albrecht et al. (2007) in 2D domains.

Numerical simulations of electrophoretic separations in microfluidic chips represent a challenging problem from the computational point of view. Both the large difference among the relevant length scales involved and the multiphysics nature of the problem, lead to numerical difficulties: multiple nonlinear problems (each field requires a nonlinear calculation), excessive number of degrees of freedom, and ill-conditioning global matrices due to the high aspect ratios. Therefore, the implementation of parallel computations and advanced preconditioning, such as domain decomposition techniques, are crucial for the achievement of accurate numerical results and low computation times. Parallel computations and domain decomposition techniques in modeling electrokinetic flow and mass transport have not been extensively explored. Tsai et al. (2005) presented a 2D parallel finite volume scheme to solve EOF in L-shaped microchannels. 3D simulations of electrophoretic processes employing parallel calculations were performed by Chau et al. (2008) for FFE using finite difference method, and by Kler et al. (2009) for CZE using FEM.

Here, a 3D and time-dependent numerical model for electrophoretic processes in microfluidic chips is presented. The model can also work in 1D and 2D geometric domains, or stationary mode. Numerical calculations are carried out by using PETSc (Portable Extensible Toolkit for Scientific Computation)-FEM, in a Python environment. The method includes a set of last generation preconditioners and solvers, especially addressed to 3D problems, which significantly improve numerical efficiency in comparison with typical software of multiphysics available for the purposes. As a matter of fact, the time required to complete the computation of a benchmark is reduced to $<30\%$, as shown in the Electronic Supplementary Material (Online Resource 1). This advantage allows one to solve full, complex microfluidic problems, such as those found in numerical prototyping of state-of-the-art electrophoresis on chips.

Precisely, it is relevant to note that 3D simulations of the complete multiphysics problem of 2DE are not available in the literature, to the best of our knowledge. The closest approach to the subject is the work from Yang et al. (2008) that considers the transport of a single component sample in a 2D domain. Our model simulates transport, separation, and detection of several components (mixtures of more than 30 species), which undergo chemical reactions, in 3D domains.

In this article, after presenting the mathematical modeling (Sect. 2), simulation tools (Sect. 3), and two validation examples (Sects. 4.1 and 4.2), the numerical prototype of an electrophoretic chip involving FFIEF and CZE is discussed (Sect. 4.3).

2 Modeling

This section describes the mathematical model. First the fluid dynamics and the electric field are discussed, then the relationship between buffer composition and physicochemical properties of the channels wall is presented, finally the mass transport balance for all species considered and the chemistry involved are described.

Isothermal conditions are assumed throughout this work. It is known that an important effect associated with electric current in microchannels is temperature rising due to internal heat generation, namely Joule effect (Li 2004). Nevertheless, if the applied electric field is relatively low, and the microfluidic chip is able to reject the heat to the environment, the fluid temperature does not change appreciably (MacInnes et al. 2003; Berli 2008; Kohlheyer et al. 2008).

2.1 Flow field

In the framework of continuum fluid mechanics, fluid velocity u and pressure p are governed by the following equations (Probstein 2003; Li 2004):

$$-\nabla \cdot \mathbf{u} = 0, \tag{1}$$

$$\rho\left(\frac{\partial u}{\partial t} + \mathbf{u}\cdot\nabla\mathbf{u}\right) = \nabla\cdot\left(-p\mathbf{I} + \mu(\nabla\mathbf{u} + \nabla\mathbf{u}^T)\right) + \rho\mathbf{g} + \rho_e\mathbf{E}. \tag{2}$$

Equation 1 expresses the conservation of mass for incompressible fluids. Equation 2 expresses the conservation of momentum for Newtonian fluids of density ρ, viscosity μ, subjected to gravitational field of acceleration g and electric field strength E. The last term on the right-hand side of Eq. 2 represents the contribution of electrical forces to the momentum balance, where $\rho_e = F\sum_j z_j c_j$ is the electric charge density of the electrolyte solution, obtained as the summation over all type-j ions, with valence z_j and concentration c_j, and F is the Faraday constant.

2.2 Electric field

The relationship between electric field and charge distributions in the fluid of permittivity ε is given by

$$\epsilon\nabla\cdot\mathbf{E} = \rho_e. \tag{3}$$

Modeling electrophoresis problems demands special considerations on the electric field, since it involves different contributions in the flow domain, and is strongly affected by the presence of non-uniform electrolyte concentrations. Here, we describe the computation of the electric field, as well the hypothesis included to simplify numerical calculations. For this purpose, a (η, τ) wall-fitted coordinate system is used, where η and τ are, respectively, the coordinates normal and tangent to the solid boundaries.

The first contribution to the electric field comes from the presence of electrostatic charges at solid–liquid interfaces. The interfacial charge has associated an electric potential ψ that decreases steeply in η-direction due to the screening produced by counterions and other electrolyte ions in solution, namely the EDL. The thickness of this layer is given by Debye length λ_D, which is on the order of 1–10 nm for the ionic concentrations commonly used in electrophoresis. The value of ψ at the plane of shear is the electrokinetic potential ζ. Also in this modeling, ζ is allowed to vary smoothly along the τ-direction (see Sect. 2.3) on a length scale L around 1 cm. Nevertheless, since $\zeta/\lambda_D \gg \zeta/L$, the variation of ψ with τ is disregarded and ψ is assumed to vary with η only.

There is also a potential ϕ in the flow domain, which comes from the potential difference $\Delta\phi$ externally applied to drive electrophoresis and/or induce EOF. As the channel walls are supposed perfectly isolating, there are no components of the applied field normal to the wall, and ϕ varies in τ-direction only.

Therefore, the total electric potential may be written as $\Phi(\eta, \tau) = \psi(\eta) + \phi(\tau)$. This superposition is valid if the EDL retains its equilibrium charge distribution when the electrolyte solution flows. The approximation is part of the standard electrokinetic model (Hunter 2001) and holds if the applied electric field ($\sim\Delta\phi/L$) is small in comparison with the EDL electric field ($\sim\zeta/\lambda_D$), which is normally the case in practice. Introducing the electric field $E = -\nabla\Phi$ into Eq. 3 leads to the following expression

$$\frac{\partial^2\psi}{\partial\eta^2} + \frac{\partial^2\phi}{\partial\tau^2} = -\frac{\rho_e}{\epsilon}. \tag{4}$$

The second term of this equation is non-null in electrophoresis problems because the presence of concentration gradients in the fluid induces a variation of $\frac{\partial\phi}{\partial\tau}$ along the channel. However, $\frac{\partial^2\phi}{\partial\tau^2}$ is several orders of magnitude lower than $\frac{\partial^2\psi}{\partial\eta^2}$ (see also MacInnes 2002; Sounart and Baygents 2007; Craven et al. 2008; Barz 2009), which allows one to split the computation of the electric field in two parts, as explained below.

2.2.1 *Electric double layer*

According to the previous analysis, the EDL potential is governed by $\frac{\partial^2\psi}{\partial\eta^2} = -\frac{\rho_e}{\epsilon}$. Introducing the ion concentrations c_j in the form of Boltzmann-type distributions yields Poisson–Boltzmann model of the diffuse layer, which enables the calculation of $\psi(\eta)$. This solution is useful to compute the EOF in nanochannels, or in microchannels with complicated geometries, such as sharp corners (Kler et al. 2009). Nevertheless, computational requirements are very large when a whole chip is modeled. In this sense, and considering that the present work focuses on electrophoretic processes, here we simplify the calculation of the EOF by introducing the so-called thin EDL approximation (Brunet and Adjari 2004; Berli 2008): electro-osmosis is regarded as an electrically induced slip velocity in the direction of the applied electric field, the magnitude of which is given by Helmholtz–Smoluchowski equation

$$\mathbf{u} = \frac{\epsilon\zeta}{\mu}\nabla\phi. \tag{5}$$

This approximation also implies that $\rho_e \approx 0$ in the fluid outside the EDL, meaning that the last term on the right-hand side of Eq. 2 is negligible. Thus, the electro-osmotic velocity enters the hydrodynamic field as a boundary condition, which significantly reduces computational demands. The simplification is appropriate taking into

account that $\lambda_D \approx 1$–10 nm, while cross-sectional channel dimensions are 10–100 μm.

2.2.2 Bulk fluid

Given the considerations made above, the electric potential $\phi(\tau)$ has to be calculated from the charge conservation equation in steady state (Probstein 2003):

$$\nabla \cdot \left(-\sigma \nabla \phi - F \sum_{j=1}^{N} z_j D_j \nabla c_j + \rho_e \mathbf{u} \right) = 0, \tag{6}$$

where D_j is the diffusion coefficient and σ is the electrical conductivity of the electrolyte solution

$$\sigma = F^2 \sum_{j=1}^{N} {z_j}^2 \Omega_j c_j, \tag{7}$$

where Ω_j is the ionic mobility. In fact, the terms between brackets in Eq. 6 constitute the electric current density i, which accounts for the ion fluxes due to fluid convection, electrical forces, and Brownian diffusion. Finally, one may note that Eq. 6 reduces to $\frac{\partial^2 \phi}{\partial \tau^2} = 0$ (Laplace equation for the applied potential) only if electrolyte concentrations and mobilities are perfectly uniform.

2.3 Electrokinetic potential

In a typical IEF assay the pH changes several units along the channel, which induces a parallel variation of ζ, provided the interfacial charge has not been fully suppressed. In order to account for the influence of this variation on the EOF, here we include a model of ζ in terms of the pH and the ionic strength $I = \frac{1}{2}\sum_j {z_j}^2 c_j$, which represents the total ion concentrations of the bulk.

The electrokinetic potential at the solid–fluid interface depends on the charge generation mechanism of the surface (Hunter 2001). In principle, it may be thought that solid walls expose toward the fluid a certain number of specific sites (n_S) able to release or take H^+ ions, with a dissociation constant K_S. In equilibrium with an aqueous electrolyte solution, the surface becomes electrically charged. For the case of interfaces containing weak acid groups, such as silanol in fused silica capillaries and carboxyl in synthetic polymer materials, the following relationship is appropriate for symmetric monovalent electrolytes (Berli et al. 2003):

$$(8\epsilon k_B T I N_A)^{(\frac{1}{2})} \sinh\left(\frac{ze\zeta}{2k_B T}\right) = \frac{-en_S}{1 + 10^{(pK_S - pH)} e^{-e\zeta/k_B T}} \tag{8}$$

Therefore, if the parameters that characterize the interface are known (n_S, K_S), the ζ-potential can be readily predicted for different values of pH and I. Then the electro-osmotic velocity is directly coupled to the electrolyte composition. Empirical formulae of ζ(pH, I) were also reported in order to simplify calculations (Kirby and Hasselbrink 2004).

2.4 Mass transport and chemistry

The mass transport of weakly concentrated sample ions and buffer electrolyte constituents can be modeled by a linear superposition of migrative, convective, and diffusive transport mechanisms, plus a source term due to chemical reactions. In a non-stationary mode, the concentration of each j-type species, is governed by (Probstein 2003):

$$\frac{\partial c_j}{\partial t} + \nabla \cdot (-z_j \Omega_j \nabla \phi c_j + \mathbf{u} c_j - D_j \nabla c_j) - r_j = 0, \tag{9}$$

where r_j is the reaction term. Different electrolytes (acids, bases, and ampholytes), analytes, and particularly the hydrogen ion have to be considered. In electrolyte chemistry the processes of association and dissociation are much faster than the transport electrokinetic processes, hence, it is a good approximation to adopt chemical equilibrium constants to model the reactions of weak electrolytes (Arnaud et al. 2002), while strong electrolytes are considered as completely dissociated.

2.4.1 Acid–base reactions

For the general case, reactions associated to an ampholyte A are

$$AH \rightleftharpoons A^- + H^+ \tag{10}$$

$$AH_2^+ \rightleftharpoons AH + H^+ \tag{11}$$

then the equilibrium state is characterized by,

$$\frac{k_{a2}}{k_{a1}} = \frac{[A^-][H^+]}{[AH]} = K_a \tag{12}$$

$$\frac{k_{b2}}{k_{b1}} = \frac{[AH][H^+]}{[AH_2^+]} = K_b, \tag{13}$$

where the square brackets represent concentration (mol/m^3) of the given specie. The corresponding expressions of r_j are obtained as follows

$$r_{A^-} = -k_{a1}[A^-][H^+] + k_{a2}[AH] \tag{14}$$

$$r_{AH} = k_{a1}[A^-][H^+] - k_{a2}[AH] - k_{b1}[AH][H^+] + k_{b2}[AH_2^+] \tag{15}$$

$$r_{AH_2^+} = k_{b1}[AH][H^+] - k_{b2}[AH_2^+] \tag{16}$$

$$r_{H^+} = -k_{a1}[A^-][H^+] + k_{a2}[AH] - k_{b1}[AH][H^+] + k_{b2}[AH_2^+] \tag{17}$$

In Eq. 17 the water dissociation term is not included due to the fact that this reaction is several orders of magnitude

faster than reactions 10 and 11 (Arnaud et al. 2002), then $[OH^-]$ can be calculated directly as

$$[OH^-] = \frac{K_w}{[H^+]}, \tag{18}$$

where $K_w = 10^{-14}$.

2.4.2 *Effective charge and mobility of analytes*

When the concentration of analytes is much lower than that of buffer constituents, its effect on the pH is negligible. In these cases, considering all ionic species represents a high computational cost. However, the influence of pH on the analytes must be taking into account. Thus, the transport equation of these analytes includes $r_j = 0$, and the product $z_j\Omega_j$ as a function of pH. For example, if the specie is an ampholyte that obeys a reaction scheme like the one shown in Eqs. 10 and 11, $z_j\Omega_j$ is included in Eq. 9 as an effective charge–mobility product ($z_{\text{eff}}(j)\Omega_{\text{eff}}(j)$; Chatterjee 2003). This product is calculated as $(\alpha_0 - \alpha_2)\Omega_j$, where $\alpha_0 = [A^-]/[A_T]$ and $\alpha_2 = [AH_2^+]/[A_T]$ with $A_T = [AH_2^+] + [AH] + [A^-]$, are the degrees of dissociation of anions and cations, respectively, which are written in terms of $[H^+]$ as

$$\alpha_0 = \frac{\frac{K_a K_b}{[H^+]^2}}{1 + \frac{K_b}{[H^+]} + \frac{K_a K_b}{[H^+]^2}} \tag{19}$$

$$\alpha_2 = \frac{1}{1 + \frac{K_b}{[H^+]} + \frac{K_a K_b}{[H^+]^2}} \tag{20}$$

Therefore, the governing equation for the sample plug results

$$\frac{\partial c_j}{\partial t} + \nabla \cdot [-(\alpha_0 - \alpha_2)\Omega_j \nabla \phi c_j + \mathbf{u} c_j - D_j \nabla c_j] = 0, \tag{21}$$

where it is observed that the physical motion of analytes is coupled to the degree of dissociation at a given pH.

Previous works (Chatterjee 2003; Shim et al. 2007) calculate the pH by using a nonlinear equation based on global electroneutrality, to avoid the solution of reactive terms and Eq. 9 for hydrogen ion. In parallel computing, solving monolithically two different nonlinear systems is discouraged due to its mathematical complexity (Storti et al. 2009) and computational inefficiency (Cai and Keyes 2002).

Finally, the reactive scheme (Eqs. 9–17) is used to solve species that change pH conditions, and the effective mobility scheme ($r_j = 0$ and Eqs. 19–21) for those that cannot affect considerably the pH conditions. This scheme provides convergence, stability, and does not affect parallel calculations performance. In addition, the scheme allows to treat different reactive schemes, as enzymatic process or antigen–antibody systems, and different mobilities models.

3 Simulation tools

3.1 Software

All numerical simulations presented were performed within a programming environment built upon *MPI for Python* (Dalcín et al. 2008), *PETSc for Python*, and *PETSc-FEM* (Sonzogni et al. 2002). PETSc-FEM is a parallel multiphysics code primarily targeted to 2D and 3D finite elements computations on general unstructured grids. PETSc-FEM is based on MPI and PETSc (Balay et al. 2008), it is being developed since 1999 at the *International Center for Numerical Methods in Engineering* (CIMEC), Argentina. PETSc-FEM provides a core library in charge of managing parallel data distribution and assembly of residual vectors and Jacobian matrices, as well as facilities for general tensor algebra computations at the level of problem-specific finite element routines. In addition, PETSc-FEM provides a suite of specialized application programs built on top of the core library but targeted to a variety of problems (e.g., compressible/incompressible Navier–Stokes and compressible Euler equations, general advective–diffusive systems, weak/strong fluid-structure interaction). In particular mass transport, chemistry and fluid flow computations presented in this article were carried out within the Navier–Stokes module available in *PETSc-FEM*. This module provides the required capabilities for simulating mass transport and incompressible fluid flow through a monolithic *SUPG/PSPG* (Tezduyar et al. 1992; Tezduyar and Osawa 2000) stabilized formulation for linear finite elements. Electric field computations were carried out with the Charge Conservation module and transport equation was solved using the Electrophoresis module. Visualization and post-processing are carried out in Paraview 3.6 (Sandia and CSimSoft 2000–2009).

In Online Resource 1, we compare the efficiency (computational time) of PETSc-FEM against a typical commercial software for multiphysics. A defined fluid dynamic problem is solved by using each method with the same hardware facilities.

3.2 Hardware

Simulations were carried out by using a Beowulf cluster *Aquiles* (Storti 2005–2008). The hardware consists of 82 disk-less single processor computing nodes with Intel Pentium 4 Prescott 3.0 GHz 2 MB cache processors, Intel Desktop Board D915PGN motherboards, Kingston Value RAM 2 GB DDR2 400 MHz memory, and 3Com 2000ct Gigabit LAN network cards, interconnected with a 3Com SuperStack 3 Switch 3870 48-ports Gigabit Ethernet.

4 Validation and application examples

In what follows, three numerical examples of different electrophoretic separations are presented: (1) a benchmark that consist in an IEF assay by immobilized pH gradient (IPG), (2) an IEF assay by ampholyte-based pH gradient, and (3) a 2DE assay involving FFIEF plus CZE. All numerical examples were solved neglecting gravitational forces, i.e., channels are supposed to be in horizontal position.

4.1 IEF by IPG

4.1.1 Stagnant fluid

In order to validate the model, an histidine IEF by IPG reported in the literature (Palusinski et al. 1986; Chatterjee 2003) is reproduced here. The aminoacid histidine is focused in a straight channel (0.1×1.0 cm^2). IPG is achieved by immobilizing cacodylic acid (CACO) and tris(hydroxymethyl)-aminoetane (TRIS). Physicochemical parameters are summarized in Table 1.

Boundary conditions: a constant current density $i = 0.2$ A m^{-2} is imposed, this condition is attained by applying an appropriate potential difference $\Delta\phi$, which is instantaneously corrected with the actual value of σ. The anode is located at the left wall ($x = 0.0$ cm) of the channel, and cathode at the right wall ($x = 1.0$ cm). The concentrations of CACO and TRIS are fixed in a linear way to obtain the pH profile, histidine flux through the up and bottom walls is set to zero.

After the IPG is established, a sample of 1 mM histidine is injected in the whole channel. Then a constant current density $i = 0.2$ A m^{-2} has to be imposed. Concentration of histidine and conductivity profiles at different times at the centre of the channel are shown in Fig. 1a, b, respectively. The conductivity profile clearly shows the effect of the histidine concentration. During the focusing process conductivity follows the histidine concentration, decreasing considerably at channel ends. As a consequence, the electric field (which is directly coupled to conductivity by Eq. 6) raise at this regions, further increasing the focusing process. Results reasonably agree with those previously reported.

Table 1 Physicochemical properties of analyte and buffer constituents (Palusinski et al. 1986; Chatterjee 2003)

Component	pK_a	pK_b	pI	Ω (m^2/V s)	D (m^2/s)
Histidine	6.04	9.17	7.50	2.02×10^{-8}	5.22×10^{-10}
CACO	6.21	–	–	0.0	0.0
TRIS	–	8.30	–	0.0	0.0

4.1.2 EOF effects

The previous example involved no bulk flow. In practice, this situation is hard to reach because the ζ-potential cannot be reduced to zero, and the resulting EOF has strong effects in focusing performance. Several attempts to quantify this effect were reported in the literature (Herr et al. 2000; Thormann et al. 2007). Here, we simulate the histidine focusing problem with bulk flow due to the presence of EOF. The magnitude of the flow is related to the local electric field, wall electric properties, and buffer solution composition, as described in Sect. 2. Calculations were carried out by using numerical values of the previous example (Table 1).

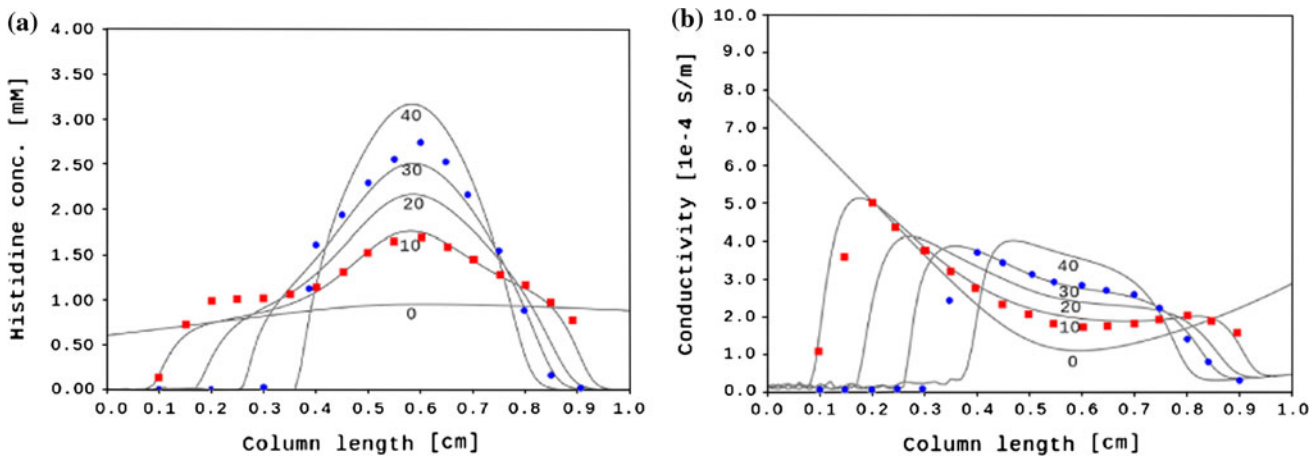

Fig. 1 Concentration and conductivity profiles along the channel at 0, 10, 20, 30, and 40 min. *Full lines* are the results of present work. *Symbols* corresponds to the values obtained by Palusinski et al. (1986); *squares* for 10 min and *circles* for 30 min. **a** Histidine concentration, **b** conductivity

Boundary conditions: apart from the conditions used in the previous example, here pressure is set to 0 Pa at the cathode, tangent velocity is set to 0 m/s at the anode and the cathode. As the calculation domain is 2D (x–y plane, see Fig. 2), the simulation implicitly assumes that the channel is considerably larger in the z direction than in the y direction. Therefore, EOF slip velocity (Eq. 5) is included as the boundary condition at planes $y = 0.0$ cm and $y = 0.1$ cm only.

In this case, due to the variation of pH along the channel, the wall ζ-potential was modeled with Eq. 8. Parameters for this equation are: $pK_S = 7.0$ and $n_S = 1.22 \times 10^{16} + 7.3 \times 10^{16}\ c_0$, where c_0 is the local ion concentration (Berli et al. 2003).

Figure 2 shows 2D plots of conductivity, electric field, pressure, and fluid velocity, 2 min after the external potential is applied. A strong coupling between these fields is observed. In fact, the fluid velocity is determined by both (i) ζ, which depends on pH and I and (ii) E which in turn depends on σ (Fig. 2a, b). The superposition of these effects generates a non-uniform fluid velocity field along the channel (Fig. 2c) and the consequent pressure gradients (Fig. 2d). These non-uniformities are well known from ITP where electric field spatial variations due to conductivity gradients are important (Thormann et al. 2007). Here, non-uniform ζ-potential effects are simulated without approximations. It is worth noting that previous works (Thormann et al. 2007; Herr et al. 2003) use an spatially averaged electro-osmotic velocity. Finally, under the conditions of this example, the influence of $E(\sigma)$ prevails. Results shown in Fig. 2 are in agreement with experiments (Herr et al. 2003) and simulations (Thormann et al. 2007) reported in the literature. Focusing efficiency decreases due to the sample dispersion (non-uniform transverse velocity profile) and the reduction of the sample residence time in the channel.

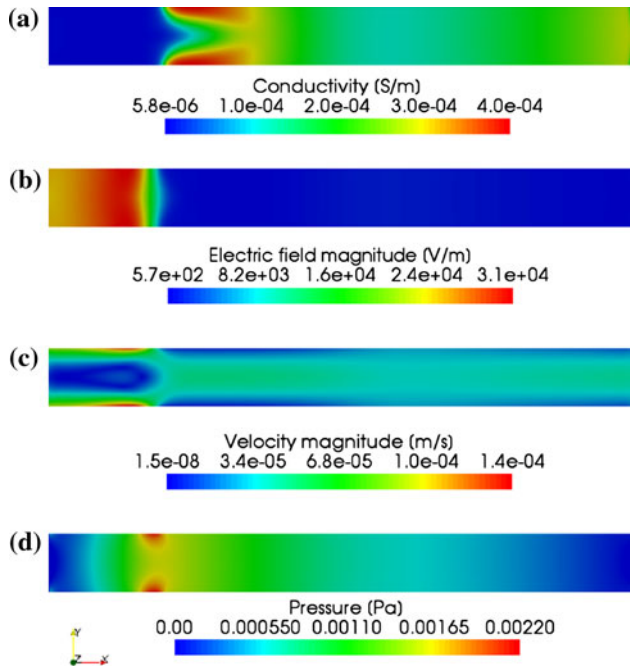

Fig. 2 **a** Conductivity, **b** electric field, **c** velocity, and **d** pressure distributions at $t = 2$ min, for IEF with EOF

4.2 IEF by ampholyte-based pH gradient

Another way to implement IEF is by using a mixture of carrier ampholytes, which naturally generates a pH gradient under the influence of an electric field. Further details on this technique can be found elsewhere (Landers 2007; Sommer and Hatch 2009). Here, we simulate an IEF assay where the pH gradient is generated by 10 ampholytes in solution. A 2D microchannel is modeled by a rectangle (0.01×1.0 cm^2). Physicochemical properties of the ampholyte (Table 2) were taken from the literature (Shim et al. 2007). Also in these calculations, $\Omega = 3 \times 10^{-8}$ m^2/V s and $D = 7.75 \times 10^{-10}$ m^2/s are used for all ampholytes. Initially ampholytes are uniformly distributed in the channel.

Boundary conditions: Potentials applied are 0 V at the cathode ($x = 0.0$ cm) and 100 V at the anode ($x = 1.0$ cm). Compounds fluxes through the walls is set to zero, except for H^+ and OH^- ions at the interfaces of anolyte and catholyte.

Figure 3a shows the pH gradient at different times, after applying the potential difference. Our predictions are compared to previous results (Fig. 3b). Unlike the IPG, ampholyte-based pH gradient has a strong transient behavior. After 80 s under the effect of the electric field, ampholytes are focused around its pI, which yield different pH steps along the channel. The step-like shape is a consequence of the reduced number of ampholytes (Svensson 1961).

Table 2 Physicochemical properties of buffer and analyte constituents

Ampholyte	pK_a	pK_b	pI
1	6.01	6.41	6.21
2	6.25	6.65	6.45
3	6.47	6.87	6.67
4	6.71	7.11	6.91
5	6.94	7.34	7.14
6	7.17	7.57	7.37
7	7.51	7.91	7.71
8	7.64	8.04	7.84
9	7.87	8.50	8.30
10	8.10	8.50	8.30

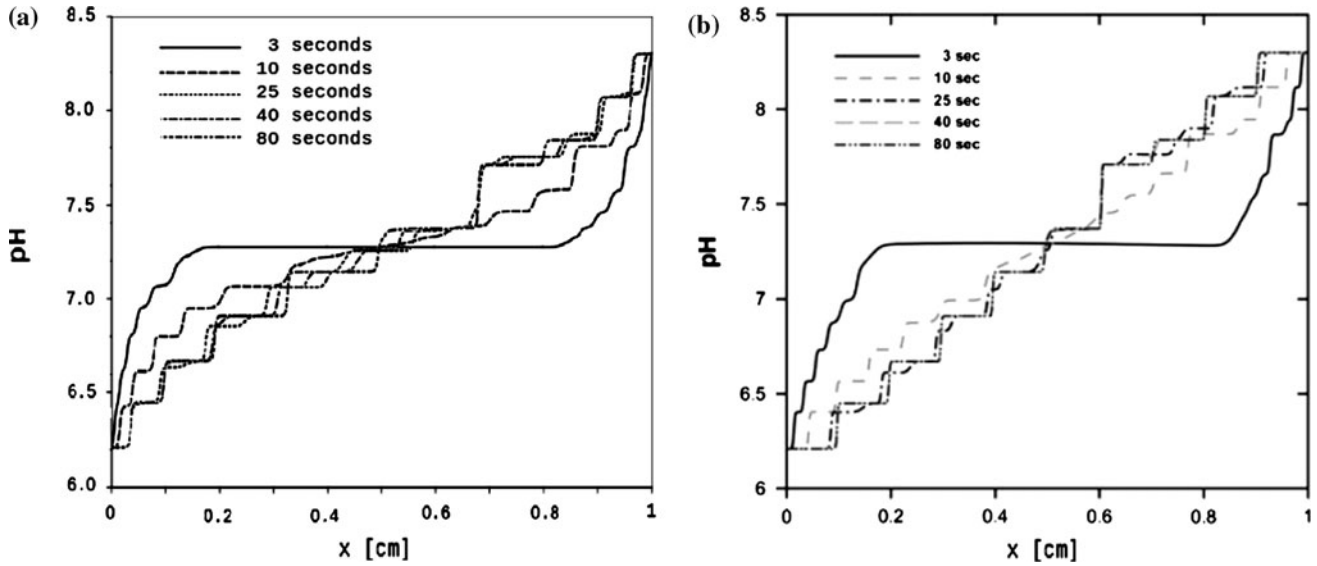

Fig. 3 pH along the centre of the channel for 3, 10, 25, 40, and 80 s. **a** Present work. **b** Shim et al. (2007). Copyright Wiley-VCH Verlag GmbH and Co. KGaA. Reproduced with permission

4.3 2DE: FFIEF + CZE

Two-dimensional electrophoretic separations consist of two independent mechanisms that are employed sequentially. The separation efficiency is estimated as the product of the independent efficiency of each method, provided the methods are uncoupled (orthogonality). IEF and CZE satisfy orthogonality and have been extensively employed in the analysis of complex protein samples in conventional devices (Herr et al. 2003). FFIEF is a derivative of FFE, a classical technique in which an electric field is applied perpendicularly to a flowing sample solution, then analytes are separated electrophoretically in a continuous flow (Xu et al. 2005; Kohlheyer et al. 2008; Turgeon and Bowser 2009). In FFIEF, a pH gradient is generated across the channel.

A 2DE separation involving FFIEF and CZE is simulated here. For this purpose, a microfluidic chip was designed following a FFIEF device recently published (Kohlheyer et al. 2006). The geometry is presented in Fig. 4. FFIEF is carried out in the FFIEF channel (103,500 × 10,000 μm^3), then samples flow through three secondary channels (10 × 600 × 10,000 μm^3), and finally CZE is developed in the CZE channel (10 × 1,000 × 50,000 μm^3). A main concern in 2DE separations is the uncoupling of the processes, which normally requires discontinuous operation in order to avoid sample dispersions, mainly due to the geometry of turns or buffer heterogeneity (Tia and Herr 2009). Here, we adopt a continuous system, in which the mentioned effects do not influence the separation performance because the number of analytes is very low compared with theoretical peak capacity of the device (Herr et al. 2003).. In addition, electric field and conductivity gradients are sufficiently low to avoid flow instabilities (Posner and Santiago 2006).

The fluid flow problem was solved by using Eqs. 1, 2, 5, and 6, and boundary conditions reported in Table 3, where $\zeta = 25$ mV. The electric potential at the initial state is shown in Fig. 4. The applied electric potentials are fixed during the operation to provide the system with: a transverse electric field in the FFIEF channel, an axial electric field in the CZE channel, and EOF in the secondary and CZE channels.

The pH gradient for FFIEF is established by focusing 20 ampholytes between two sheath flows of anolyte and catholyte, at pH 5.0 and 6.21, respectively. In these calculations, $\Omega = 3 \times 10^{-8}$ m^2/V s and $D = 7.75 \times 10^{-10}$ m^2/s are used for all ampholytes. Other physicochemical properties of buffer components are listed in Table 4. Ampholytes 1–6 were injected continuously from inlet 1, ampholytes 7–14 from inlet 2, and ampholytes

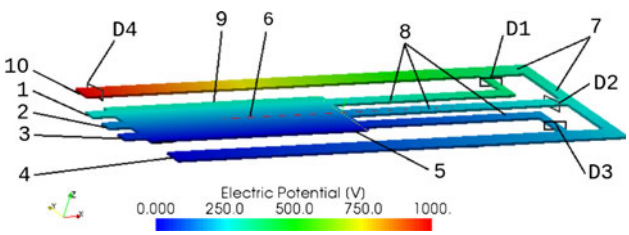

Fig. 4 Geometry and electric potential distribution for initial state. *1* inlet 1, *2* inlet 2, *3* inlet 3, *4* inlet 4 (CZE buffer inlet), *5* basic sheath flow, *6* FFIEF channel, *7* ECZ channels, *8* secondary channels, *9* acidic sheath flow, and *10* outlet. *D1, D2, D3*, and *D4*, are the locations for hypothetical detectors

Table 3 Boundary conditions for the electric field and fluid flow problems

Boundary section	Boundary condition	Value	Units
Basic sheath flow	Electric potential	300	V
Acidic sheath flow	Electric potential	0	V
Inlet 4	Electric potential	0	V
Outlet	Electric potential	1,000	V
Inlet 1–4	Pressure	0	Pa
Inlet 1–4	Tangent velocity	0	m/s
Secondary channels	Slip velocity	$-\frac{\epsilon\zeta}{\mu}\nabla\phi$	m/s
CZE channels	Slip velocity	$-\frac{\epsilon\zeta}{\mu}\nabla\phi$	m/s
Basic sheath flow	Normal velocity	0	m/s
Acidic sheath flow	Normal velocity	0	m/s
Outlet	Tangent velocity	0	m/s

15–20 from inlet 3 with a concentration of 1.0 mM. A more concentrated buffer (100 mM) at pH 4 is injected continuously from inlet 4. When ampholytes reach the CZE channel, they dilute into the buffer preserving pH 4. Stationary conditions are reached after 120 s, where a linear-like pH gradient is formed (Fig. 5).

The separation of a mixture of 9 amphoteric compounds was simulated. Physicochemical properties of these analytes (see Table 5) were selected considering the mobilities and p*I*s of human aminoacids. All analytes were injected during 1.0 s from inlet 2 with a concentration of 0.1 mM.

Table 4 Physicochemical properties of buffer constituents

Ampholyte	pK_a	pK_b	pI
1	4.90	5.30	5.10
2	4.95	5.35	5.15
3	5.00	5.40	5.20
4	5.05	5.45	5.25
5	5.10	5.50	5.30
6	5.15	5.55	5.35
7	5.20	5.60	5.40
8	5.25	5.65	5.45
9	5.30	5.70	5.50
10	5.35	5.75	5.55
11	5.40	5.80	5.60
12	5.45	5.85	5.65
13	5.50	5.90	5.70
14	5.55	5.95	5.75
15	5.60	6.00	5.80
16	5.65	6.05	5.85
17	5.70	6.10	5.90
18	5.75	6.15	5.95
19	5.80	6.20	6.00
20	5.85	6.25	6.05

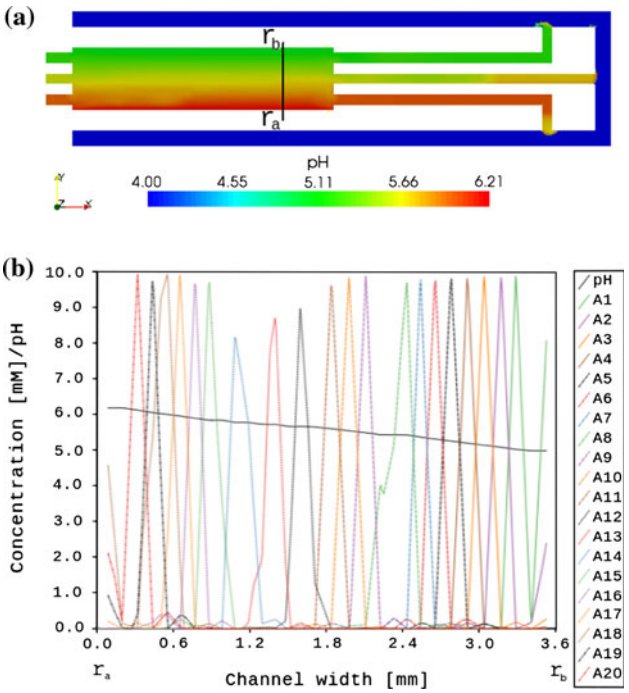

Fig. 5 **a** pH in stationary conditions at $z = 5.0$ μm. **b** Ampholyte concentration and pH across the line $r_a - r_b$ at $x = 8.0$ mm; $z = 5.0$ μm

Complete separation is achieved after 1,000 s (real time). The computational time taken to complete the simulation is 40 h. Analyte distributions during separation processes at different times are shown in Fig. 6.

A two-dimensional map of the separation is obtained from the information provided by the four hypothetical detectors shown in Fig. 4. Detector 4 acquires the entire output signal (Fig. 7a), which is sectioned in three parts. These parts are obtained taking into account signals from detectors 1 to 3, and assuming that areas under graphics are conserved. The first part of the signal has the same area that the signal of detector 1 and is assigned to the first pH range (5–5.4). The other parts of the signal are assigned to second

Table 5 Physicochemical properties of analyte constituents

Amphoteric analyte	pK_a	pK_b	pI	Ω (m^2/V s)	D (m^2/s)
1	3.22	6.88	5.09	2.64×10^{-8}	6.82×10^{-10}
2	3.65	6.72	5.18	2.84×10^{-8}	7.34×10^{-10}
3	3.70	6.80	5.25	3.84×10^{-8}	9.92×10^{-10}
4	4.12	7.03	5.57	2.24×10^{-8}	5.79×10^{-10}
5	3.96	7.26	5.61	3.18×10^{-8}	8.22×10^{-10}
6	4.18	7.26	5.72	2.45×10^{-8}	6.83×10^{-10}
7	4.17	7.30	5.73	2.17×10^{-8}	5.60×10^{-10}
8	4.32	7.59	5.95	2.41×10^{-8}	6.22×10^{-10}
9	4.33	7.58	5.95	2.24×10^{-8}	5.79×10^{-10}

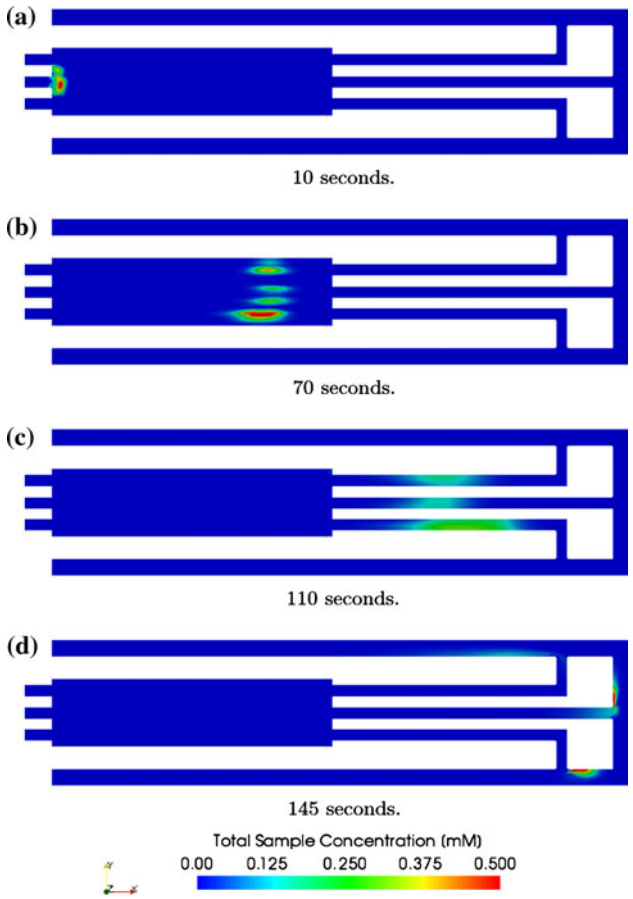

Fig. 6 Total sample distribution at 10, 70, 110, and 145 s

and third pH ranges, respectively (5.4–5.8 and 5.8–6.2). The resulting plot is shown in Fig. 7b. It is observed that the results of the numerical model can be easily presented in the graphic format that is customarily used in experiments of 2DE (Tia and Herr 2009).

5 Summary and conclusions

A 3D and time-dependent mathematical model for electrophoretic separations in microfluidic devices is presented. The model takes into account physicochemical property variations of buffer components and analytes, and its effects on fluid–solid interfaces, electric field and velocity profiles. Numerical implementation of the model is carried out by using FEM with parallel computing techniques, giving a powerful tool for simulations of electrophoretic separations in microfluidic chips.

In order to check the model, an IEF assay by IPG was simulated. Results agree with those previously reported (Palusinski et al. 1986). EOF effects in IEF assays were also analyzed. The model considers the coupling between buffer composition, flow field, electric field, and interface property variations due to the electrolyte composition. Simulation of IEF by ampholyte-based pH gradient was also made as a second validation example. The predictions of the model successfully match previous results (Shim et al. 2007).

In all cases the method is much more efficient than similar software available commercially (Online Resource 1).

Finally, a 2DE was simulated: the separation of nine amphoteric compounds by means of FFIEF and CZE was studied. The successful simulation of this complex system (3D, time-dependant, high aspect ratios in geometry,

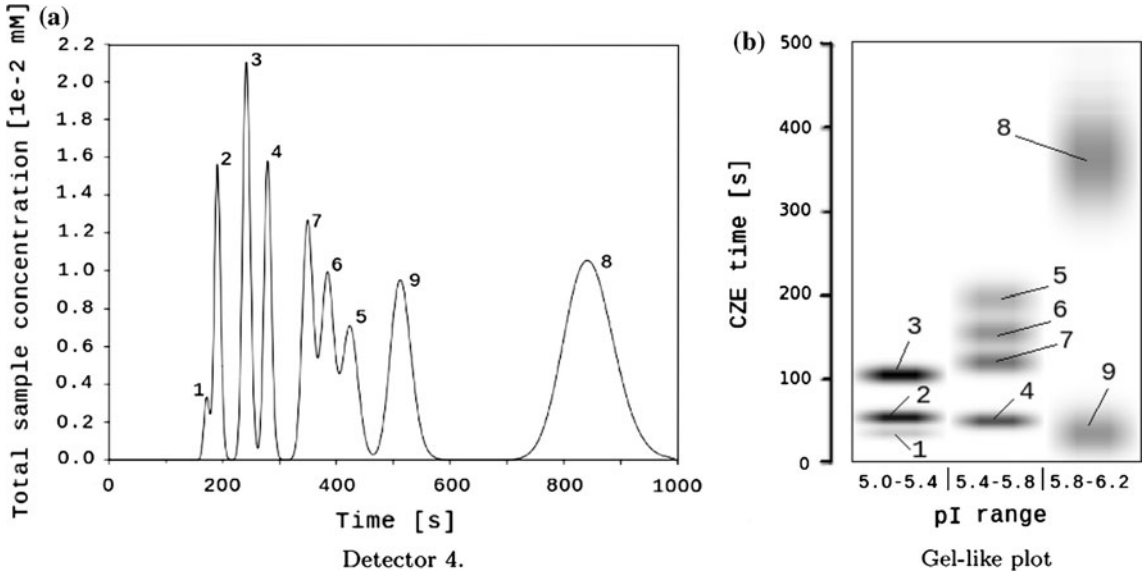

Fig. 7 **a** Detector 4 signal. **b** Gel-like plot of the two-dimensional separation (FFIEF + CZE). Numbers 1–9 refer to analytes using denominations employed in Table 5

nonlinear fields) denotes the capability of the model to test and design state-of-the-art electrophoretic chips. Such a numerical prototyping of 2DE had not been reported before in the literature.

Acknowledgements This work has received financial support from Consejo Nacional de Investigaciones Científicas y Técnicas (CONICET, Argentina), Universidad Nacional del Litoral (UNL, Argentina) and Agencia Nacional de Promoción Científica y Tecnológica (ANPCyT, Argentina). Authors made extensive use of freely distributed software as GNU/Linux OS, MPI, PETSc, GCC compilers, Paraview, Python, VTK, among many others.

References

Albrecht JW, El-Ali J, Jensen KF (2007) Cascaded free-flow isoelectric focusing for improved focusing speed and resolution. Anal Chem 79:9364–9371

Arnaud I, Josserand J, Rossier J, Girault H (2002) Finite element simulation of off-gel buffering. Electrophoresis 23:3253–3261

Balay S, Buschelman K, Gropp WD, Kaushik D, Knepley MG, McInnes LC, Smith BF, Zhang H (2008) PETSc Web page. http://www.mcs.anl.gov/petsc

Barz DP (2009) Comprehensive model of electrokinetic flow and migration in microchannels with conductivity gradients. Microfluid Nanofluid 7(2):249–265

Bercovici M, Lele SK, Santiago JG (2009) Open source simulation tool for electrophoretic stacking, focusing, and separation. J Chromatogr A 1216:1008–1018

Berli CLA (2008) Equivalent circuit modeling of electrokinetically driven analytical microsystems. Microfluid Nanofluid 4(5):391–399

Berli CLA, Piaggio M, Deiber J (2003) Modeling the zeta potential of silica capillaries in relation to the background electrolyte composition. Electrophoresis 24:1587–1595

Bianchi F, Ferrigno R, Girault H (2000) Finite element simulation of an electroosmotic-driven flow division at a T-junction of microscale dimensions. Anal Chem 72(9):1987–1993

Brunet E, Adjari A (2004) Generalized Onsager relations for electrokinetic effects in anisotropic and heterogeneous geometries. Phys Rev E 69(1):016,306

Cai XC, Keyes DE (2002) Nonlinearly preconditioned inexact newton algorithms. SIAM J Sci Comput 24(1):183–200

Chatterjee A (2003) Generalized numerical formulations for multiphysics microfluidics-type applications. J Micromech Microeng 13:758–767

Chau M, Spiteri P, Guivarich R, Boisson H (2008) Parallel asynchronous iterations for the solution of a 3d continuous flow electrophoresis problem. Comput Fluid 37(9):1126–1137

Craven TJ, Rees JM, Zimmerman WB (2008) On slip velocity boundary conditions for electroosmotic flow near sharp corners. Phys Fluids 20(4):043,603

Dalcín L, Paz R, D'Elia MSJ (2008) MPI for Python: performance improvements and MPI-2 extensions. J Parallel Distr Comput 68(5):655–662

Erickson D (2005) Towards numerical prototyping of labs-on-chip: modeling for integrated microfluidic devices. Microfluid Nanofluid 1(4):301–318

Ermakov S, Jacobson S, Ramsey J (1998) Computer simulations of electrokinetic transport in microfabricated channel structures. Anal Chem 70(21):4494–4504

Ermakov S, Jacobson S, Ramsey J (2000) Computer simulations of electrokinetic injection techniques in microfluidic devices. Anal Chem 72(15):3512–3517

Herr A, Molho J, Santiago J, Mungal M, Kenny T, Garguilo M (2000) Electroosmotic capillary flow with nonuniform zeta potential. Anal Chem 72:1053–1057

Herr A, Molho J, Drouvalakis K, Mikkelsen J, Utz P, Santiago J, Kenny T (2003) On-chip coupling of isoelectric focusing and free solution electrophoresis for multidimensional separations. Anal Chem 75:1180–1187

Hruska V, Jaros M, Gas B (2006) Simul 5—free dynamic simulator of electrophoresis. Electrophoresis 27:984–991

Hunter R (2001) Foundations of colloid science, 2nd edn. Oxford University Press, Oxford

Kirby BJ, Hasselbrink EF Jr (2004) Zeta potential of microfluidic substrates: 1. theory, experimental techniques, and effects on separations. Electrophoresis 25:187–202

Kler PA, López EJ, Dalcín LD, Guarnieri FA, Storti MA (2009) High performance simulations of electrokinetic flow and transport in microfluidic chips. Comput Method Appl M 198(30–32):2360–2367

Kohlheyer D, Besselink GAJ, Schlautmann S, Schasfoort RBM (2006) Free-flow zone electrophoresis and isoelectric focusing using a microfabricated glass device with ion permeable membranes. Lab Chip 6:374–380

Kohlheyer D, Eijkel JCT, van den Berg A, Schasfoort RBM (2008) Miniaturizing free-flow electrophoresis a critical review. Electrophoresis 29(5):977– 993

Landers JP (2007) Handbook of capillary and microchip electrophoresis and associated microtechniques, 3rd edn. CRC Press, Boca Raton

Li D (2004) Electrokinetics in microfluidics. Elsevier Academic Press, Amsterdam

MacInnes JM (2002) Computation of reacting electrokinetic flow in microchannel geometries. Chem Eng Sci 57(21):4539–4558

MacInnes J, Du X, Allen R (2003) Prediction of electrokinetic and pressure flow in a microchannel T-junction. Phys Fluids 15(7):1992–2005

Manz A, Graber N, Widmer H (1990) Miniaturized total chemical analysis systems: a novel concept for chemical sensing. Sensor Actuators B 1:244–248

Palusinski O, Graham A, Mosher R, Bier M, Saville D (1986) Theory of electrophoretic separations. part ii: construction of a numerical scheme and its applications. AICHE J 32(2):215–223

Patankar N, Hu H (1998) Numerical simulation of electroosmotic flow. Anal Chem 70(9):1870–1881

Peng Y, Pallandre A, Tran NT, Taverna M (2008) Recent innovations in protein separation on microchips by electrophoretic methods. Electrophoresis 29(1):157–178

Posner JD, Santiago JG (2006) Convective instability of electrokinetic flows in a cross-shaped microchannel. J Fluid Mech 555(1):1–42

Probstein R (2003) Physicochemical hydrodynamics. An introduction, 2nd edn. Wiley-Interscience, New York

Reyes D, Iossifidis D, Auroux P, Manz A (2002) Micro total analysis systems. 1. introduction, theory, and technology. Anal Chem 74(12):2623–2636

Sandia NL, CSimSoft (2000–2009) Paraview: large data visualiztion. http://www.paraview.org/

Saville D, Palusinski O (1986) Theory of electrophoretic separations. part i: formulation of a mathematical model. AICHE J 32(2):207–214

Shim J, Dutta P, Ivory C (2007) Modeling and simulation of IEF in 2-D microgeometries. Electrophoresis 28:572–586

Sommer G, Hatch A (2009) IEF in microfluidic devices. Electrophoresis 30:742–757

Sonzogni VE, Yommi AM, Nigro NM, Storti MA (2002) A parallel finite element program on a Beowulf cluster. Adv Eng Softw 33(7–10):427–443

Sounart TL, Baygents JC (2007) Lubrication theory for electro-osmotic flow in a non-uniform electrolyte. J Fluid Mech 576(1):139–172

Storti MA (2005–2008) Aquiles cluster at CIMEC. http://www.cimec.org.ar/aquiles

Storti MA, Nigro NM, Paz RR, Dalcín LD (2009) Strong coupling strategy for fluid–structure interaction problems in supersonic regime via fixed point iteration. J Sound Vib 320(4–5):859–877

Svensson H (1961) Isoelectric fractionation, analysis, and characterization of ampholytes in natural pH gradients. I. The differential equation of solute concentrations at steady state and its solution for simple cases. Acta Chem Scand 15:325–341

Tezduyar T, Osawa Y (2000) Finite element stabilization parameters computed from element matrices and vectors. Comput Method Appl M 190(3–4):411–430

Tezduyar T, Mittal S, Ray S, Shih R (1992) Incompressible flow computations with stabilized bilinear and linear equal order interpolation velocity pressure elements. Comput Method Appl M 95:221–242

Thormann W, Caslavska J, Mosher R (2007) Modeling of electroosmotic and electrophoretic mobilization in capillary and microchip isoelectric focusing. J Chromatogr A 1155(2):154–163

Tia S, Herr A (2009) On-chip technologies for multidimensional separations. Lab Chip 9:2524–2536

Tian WC, Finehout E (2008) Microfluidics for biological applications, 1st edn. Springer, Berlin

Tsai WB, Hsieh CJ, Chieng CC (2005) Parallel computation of electroosmotic flow in L-shaped microchannels. In: Sixth world congress of structural and multiisciplinary optimization, pp 4971–4980

Turgeon RT, Bowser MT (2009) Micro free-flow electrophoresis: theory and applications. Anal Bioanal Chem 394(1):187–198

Wu D, Qin J, Lin B (2008) Electrophoretic separations on microfluidic chips. J Chromatogr A 1184(1–2):542–559

Xu Y, Zhang CX, Janasek D, Manz A (2005) Sub-second isoelectric focusing in free flow using a microfluidic device. Lab Chip 3:224–227

Yang S, Liu J, DeVoe DL (2008) Optimization of sample transfer in two-dimensional microfluidic separation systems. Lab Chip 8:1145–1152